

Numerical Simulation of the Bottom Hole Flow Field of Particle Impact Drilling

ZHAO Jian^{[a],*}; XU Yiji^[a]; REN Jianhua^[a]; HOU Deju^[a]

^[a] College of Petroleum Engineering, China University of Petroleum, Qingdao, China.

*Corresponding author.

Received 12 October 2014; accepted 5 December 2014
Published online 29 December 2014

Abstract

It is very difficult to obtain the bottom hole fluid field of particle impact drilling through theoretical and experimental method. A method of numerical simulation was used to study the bottom hole fluid field of particle impact drilling, and it has been proved a good way to interpret particle impact process. The numerical model and computing method was used for solve the problem. It was predicted that five fluid areas were in the bottom hole fluid field by the simulation results. The changed law of the bottom hole pressure field and velocity field by altering different parameter was worked out, and the motion curve of the particles was also obtained. The result of the numerical simulation can provided more material for increasing the efficiency of particle impact and optimizing the bottom hole fluid field of particle impact drilling.

Key words: Bottom hole fluid field; Numerical simulation; Pressure and velocity field; Numerical model; Particle impact

Zhao, J., Xu, Y. J., Ren, J. H., & Hou, D. J. (2014). Numerical simulation of the bottom hole flow field of particle impact drilling. *Advances in Petroleum Exploration and Development*, 8(2), 18-23. Available from: URL: <http://www.cscanada.net/index.php/aped/article/view/5955>
DOI: <http://dx.doi.org/10.3968/5955>

INTRODUCTION

In hard formation, slow drilling speed causes long drilling cycle and higher cost, so as to further restrict the

development of the oil field^[1-4]. It is of great significance that developing new rock breaking drilling technology to promote efficient exploit of oil field^[5]. At present, new technology and new methods of improving deep well drilling speed mainly include: Developing or optimizing suitable rock breaking tools using for hard formation^[6]; Underground pressurization equipment^[7]; Using ultra-high pressure jet^[4], laser rock breaking^[8] and other new technology.

Particle impact drilling technology (PID) is one of the most efficient new technologies of rock breaking^[9]. Inspired by the projectile shock rock breaking thought, Particle Drilling Technologies INC applied it in drilling engineering field to improve the efficiency of rock breaking and rate of penetration (ROP)^[10]. In order to make full use of the particle impact drilling technology, a good understanding of the flow characteristics is necessary. Under the laboratory condition, it is difficult to directly measure the flow field characteristics. So in this paper, based on theoretical models, numerical simulations and analysis are effective^[11-12]. Based on the simulated results, some significant conclusions are obtained, which can serve as a useful reference for the optimization of the bit structure.

1. MATHEMATICAL MODEL AND NUMERICAL METHOD

1.1 Governing Equations

In order to facilitate the theory analysis and numerical simulation, simplified the space structure between the bottom and bit. As follows: (a) Assuming the produced bottom is smooth plane; (b) Surface cutting teeth are ignored; (c) The surface of bit body parallel to the bottom; (d) Using water replaces drilling mud, and the change of fluid density is also ignored^[13-19].

The standard model turbulence model is used, where Boussinesq assumption can simplify the calculation.

The equation of continuity

$$\frac{\partial u}{\partial x} + \frac{\partial v}{\partial y} + \frac{\partial w}{\partial z} = 0 \quad (1)$$

The equation of momentum

$$\frac{\partial}{\partial x_i}(\rho u_i u_j) = -\frac{\partial P}{\partial x_i} + \frac{\partial(\eta \frac{\partial u_i}{\partial x_j} - \overline{\rho u_i' u_j'})}{\partial x_j} \quad i, j=1,2,3, \quad (2)$$

The turbulent kinetic energy and the dissipation rate can be obtained by the following equations:

$$\rho u_j \frac{\partial k}{\partial x_j} = \frac{\partial}{\partial x_j} \left[\left(\eta + \frac{\eta_t}{\sigma_k} \right) \frac{\partial k}{\partial x_j} \right] + \eta_t \frac{\partial u_i}{\partial x_j} \left(\frac{\partial u_i}{\partial x_j} + \frac{\partial u_j}{\partial x_i} \right) - \rho \varepsilon \quad (3)$$

$$\rho u_j \frac{\partial \varepsilon}{\partial x_j} = \frac{\partial}{\partial x_j} \left[\left(\eta + \frac{\eta_t}{\sigma_\varepsilon} \right) \frac{\partial \varepsilon}{\partial x_j} \right] + \frac{c_1 \varepsilon}{k} \eta_t \frac{\partial u_i}{\partial x_k} \left(\frac{\partial u_i}{\partial x_k} + \frac{\partial u_k}{\partial x_i} \right) - \frac{c_2 \rho \varepsilon^2}{k} \quad (4)$$

In Equation (3) and Equation (4), η_t means the viscosity coefficient.

$$\eta_t = c_\mu \rho \frac{k^2}{\varepsilon} \quad (5)$$

In Equation (4), $c_1 = 1.44$, $c_2 = 1.92$, $c_\mu = 0.09$. Prandtl's numbers of the turbulent kinetic energy and the dissipation rate are $\sigma_k = 1.0$, $\sigma_\varepsilon = 1.3$.

1.2 Particle Track Model

The particle track model uses discrete phase to calculate. The calculation model needs some physical parameters: Initial position, velocity, particle size, temperature and so on. According to the particle force equilibrium, the motion equation in Lagrangian coordinate is obtained:

$$\frac{du_p}{dt} = F_D(u - u_p) + g_x(\rho_p - \rho) / \rho_p + F_x \quad (6)$$

Where

$$F_D = \frac{18\mu}{\rho_p D_p^2} \frac{C_D Re}{24} \quad (7)$$

Re means relative Reynolds number.

$$Re = \frac{\rho D_p |u_p - u|}{\mu} \quad (8)$$

C_D means the coefficient of resistance.

$$C_D = \alpha_1 + \frac{\alpha_2}{Re} + \frac{\alpha_3}{Re^2} \quad (9)$$

α_1 , α_2 and α_3 are constants, which are obtained through experimental results.

1.3 Calculation Model

Through the analysis of the structure of PID bit, the simplified model is established. The inner diameter of borehole is 120 mm. The bit height is 340 mm. The

distance between bit and bottom is 50 mm and the distance from side wall is 12 mm, as shown in Figure 1.

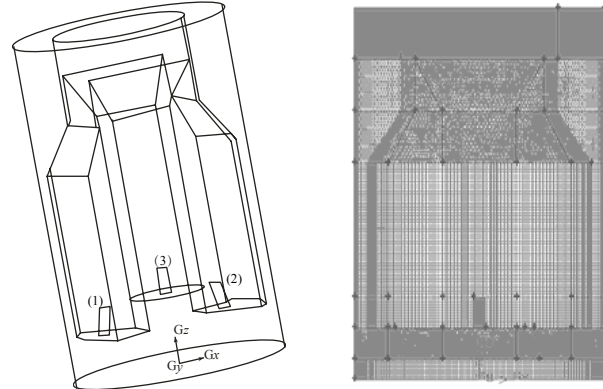


Figure 1
Three-Dimensional Simplified Diagram of PID Bit

Based on the analysis of grid generation, structured grid technology is used. The bit is divided into several pieces. Each piece uses unstructured grid. From top to bottom, the size of grid is decreased in turn, and increasing the density of grid. Because the change gradient of the nozzle and bottom is bigger, it needs a local encryption region.

Table 1
Nozzle Parameters of PID Bit

| Serial number | Nozzle diameter (mm) | Jet angle (°) | Azimuth angle (°) | Distance to the bit center (mm) |
|---------------|----------------------|---------------|-------------------|---------------------------------|
| 1 | 12 | 10 | 153 | 63 |
| 2 | 12 | 14 | -27 | 83 |
| 3 | 14 | 20 | 101 | 33 |

1.4 Boundary Conditions

The fluid boundary is the inlet of three nozzles. In the drilling process, drilling fluid with steel particles ejects at the same speed with different angles. The annular cross between the bit and the wall is the outlet boundary for the flow field. The speed and pressure of outlet are not considered. The wall boundary is obtained through the wall function method. The parameters of the first control volume which is near the wall are determined by the single wall function. The dimensionless velocity distribution of near wall obeys the logarithmic distribution:

$$U_{+p} = \frac{1}{k} \ln(Ey_{+p}) \quad (10)$$

$$y_{+p} = \frac{C_\mu^{1/4} k_p^{1/2} y_p}{v} \quad (11)$$

$$\mu_t = y_{+p} \frac{\mu}{\ln(Ey_{+p}) / k} \quad (12)$$

In order to ensure its logarithmic distribution law, y_{+p} needs to meet Equation (13):

$$11.5 \sim 30 \leq y_{+p} \leq 200 \sim 400 \quad (13)$$

2. RESULT ANALYSIS

After iterative calculation, observe the residuals surveillance curve. The results converge. And then, the discrete phase parameters are set. The model chooses steel particle as discrete phase. The volume fraction is 2%^[20]. The velocity distribution, which is related to the efficiency of rock breaking, bottom hole cleaning and wall

stabilization, is an important indicator in the study. The pressure distribution of flow field is very necessary. The study will be based on the velocity distribution and the pressure distribution.

2.1 The Velocity Distribution of Flow Field

Through simulation, the nozzle vertical interface velocity contours and vectors are shown as below:

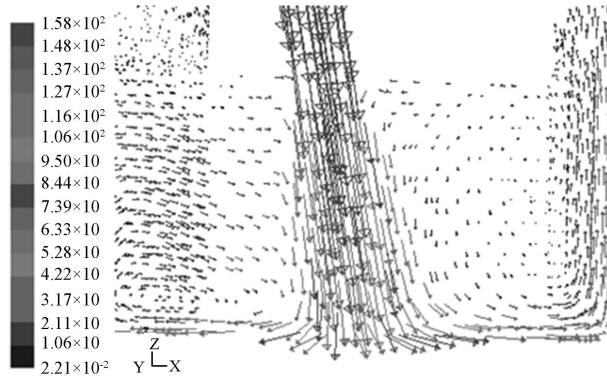
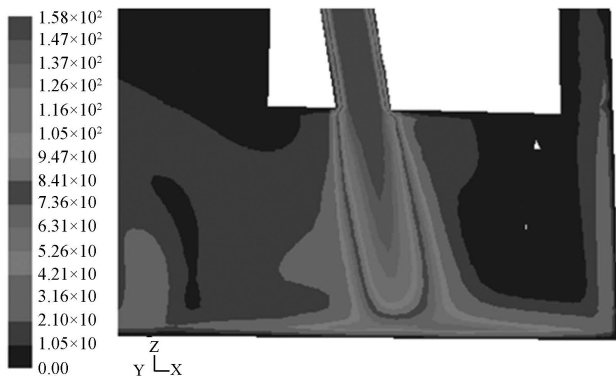


Figure 2
Jet Velocity Contour and Vector of Nozzle 1

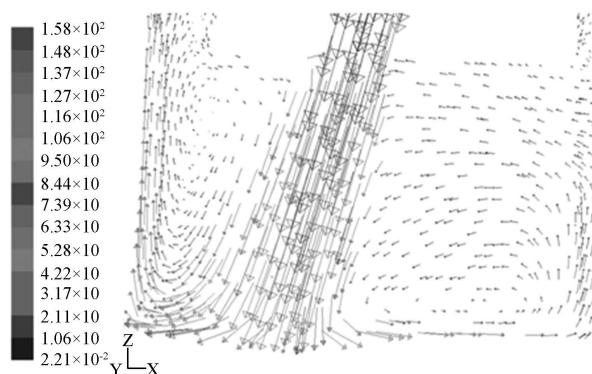
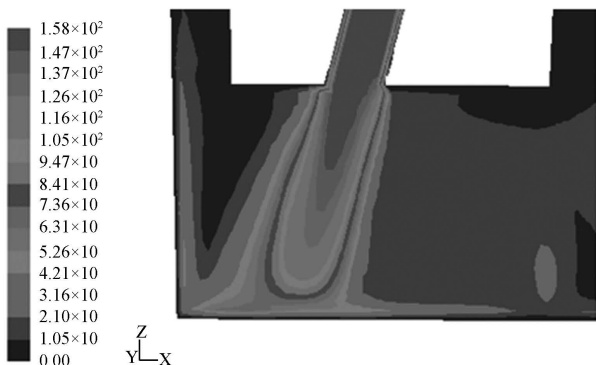


Figure 3
Jet Velocity Contour and Vector of Nozzle 2

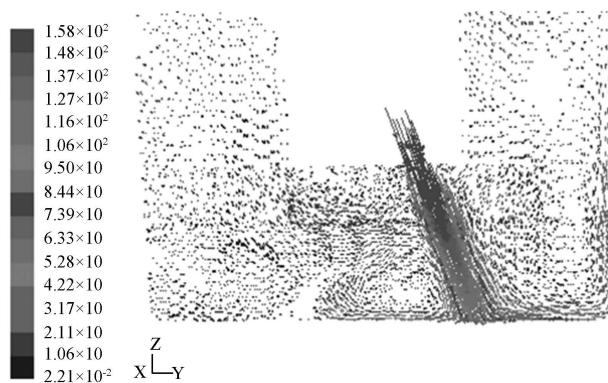
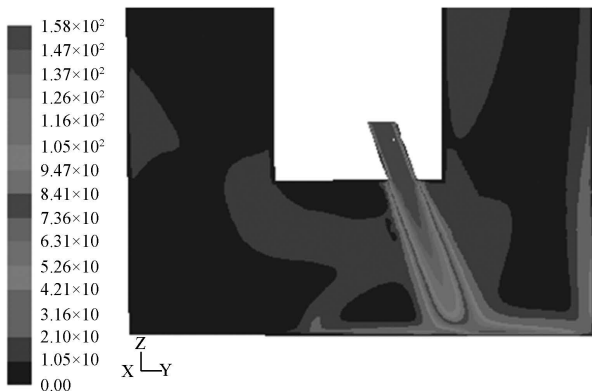


Figure 4
Jet Velocity Contour and Vector of Nozzle 3

From the analysis, the structure of the flow field can be roughly divided into five parts: Free jet area, impact area, overflow area, return area and vortex area.

2.1.1 Jet Velocity Field Analysis

In the region near the nozzle, fluid velocity is constant, named constant speed area. When the jet continues to flow, speed will reduce quickly. This is because the jet does not fully contact with the bottom and momentum exchange is less. With the movement, dramatic momentum exchange happens and the turbulent diffusion phenomenon emerges. Constant speed area no longer exists. Impact area becomes big and the radial and axial jet velocity decreases. The radial velocity decreases faster.

2.1.2 Overflow Velocity Field Analysis

When the jet impacts with the bottom, jet direction changes from the nozzle axial into the horizontal direction. This is overflow field at the bottom of well. Because of the existence of overflow field, the cuttings receive a horizontal force, which is good for cleaning the borehole^[14].

2.1.3 Return Velocity Field Analysis

When the overflow arrives at the wall, part fluid moves upward. This is return area. The majority of the fluid flows out from the outlet. Under the influence of the backflow and jet entrainment, some fluid flows into the vortex area.

From the Figures 2, 3 and 4, it can be seen that the jet height of nozzle 1 is less than that of nozzle 2 and the backflow phenomenon of nozzle 1 is evident, which means that the nozzle 2 is close to the wall and large injection angle is good for lifting.

2.1.4 Vortex Velocity Field Analysis

Because of the limit of bottom and wall, there are two vortex areas. One exists between free jet and wall. The other is between the free jet and axis of bit. The jet impacts with the bottom forming overflow, and then flows along the wall forming return area, and then flows into the annular space. In this process, the fluid of the bottom drove by the submerged jet forms vortex area.

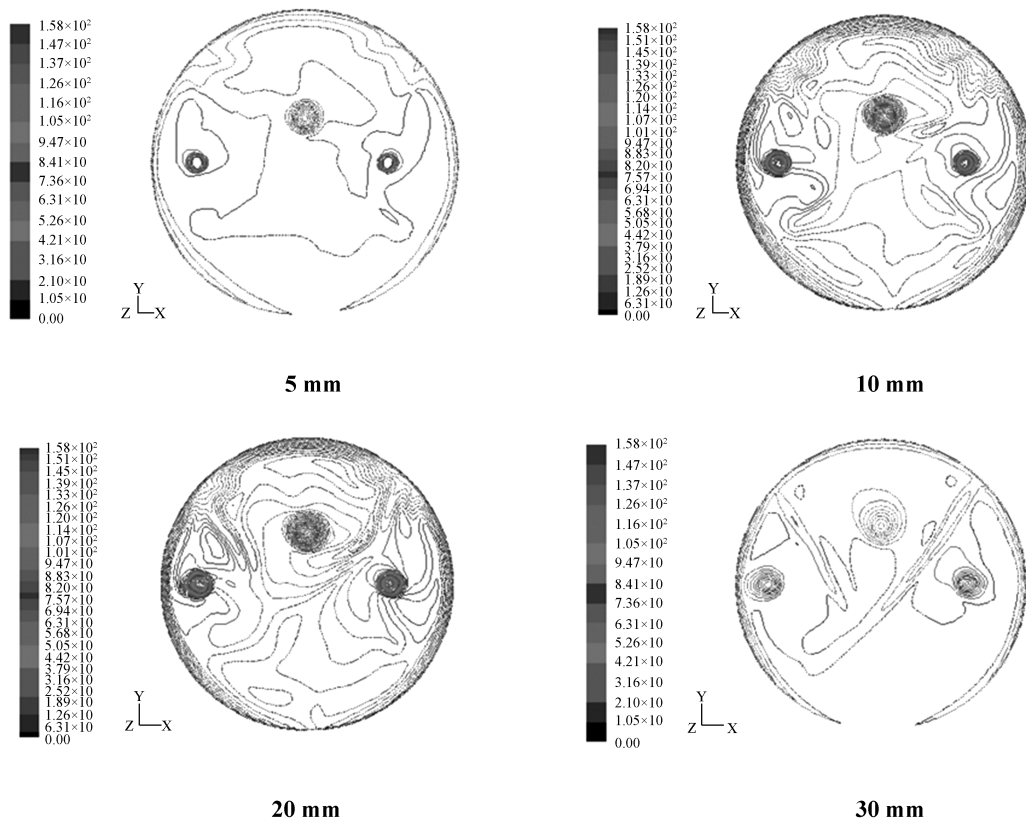


Figure 5
The Influence of Distance on the Velocity Field

2.1.5 The Influence of Distance on the Velocity Field

With the increase of the nozzle distance, the jet velocity at the center of nozzle gradually reduces. When the distance is 5 mm, the jet does not fully develop. Therefore, the velocity is large, but the impact area is lesser. 10 mm and 20 mm, attenuation of jet velocity is small and impact

area increases. When the distance is 30 mm, attenuation of jet velocity is quite obvious and the impact area increases more. It can be seen from that there must be a best distance, which can satisfy the need of speed, and also can cause the impact area as big as possible in order to get the best rock breaking effect.

2.2 Pressure Distribution

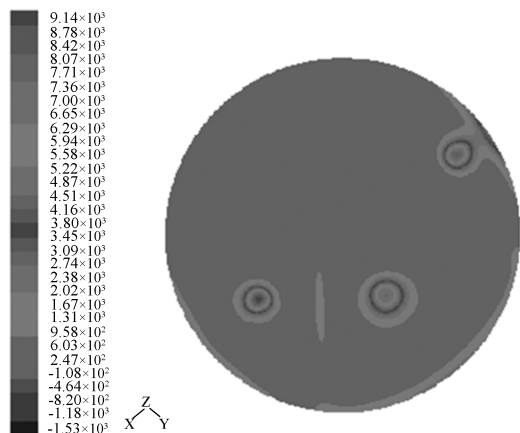


Figure 6
Pressure Contour Diagram of Bottom Cross Section

2.2.1 Characteristics of Bottom Hole Pressure

The pressure of the center of the high-speed jet is high. Because the jet mixes strongly with the surrounding media, the radial pressure attenuates quickly. In the Figure 6, central pressure of nozzle 1 is the biggest; the high pressure area of nozzle 3 is the largest. The results show that the smaller the injection angle is, the larger the central pressure is, and the smaller the high pressure area is.

2.2.2 The Effect of High-Speed Jet on the Pressure Field

The high speed jet generates high pressure area. The jet energy mostly focuses on the center of the nozzle. The radial pressure gradient is much bigger than that of normal jet. For lower strength rock, high pressure jet can directly break rock. For high strength rock, particle impacts the rock producing micro cracks and gap. At the same time, the high pressure fluid enters into the rock crack forming “water wedge”, which reduces the rock strength and greatly improves the efficiency of rock breaking^[21].

2.2.3 The Effect of Jet Angle on Pressure Field

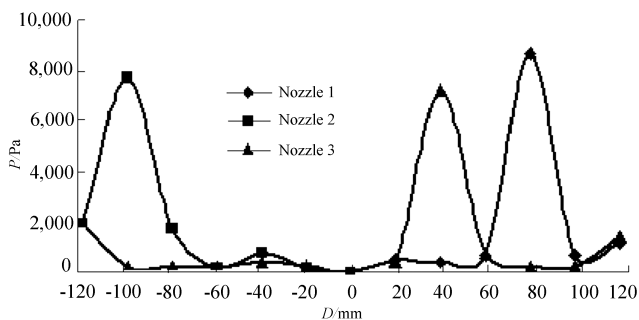


Figure 7
Radial Pressure Distribution of Nozzles

Figure 7 shows the radial pressure distribution of nozzles. As can be seen from the figures, with the increase of jet angle, the maximum of bottom pressure reduces and the impact area expands. The main reason is that: when the injection angle increases, the vertical velocity reduces and the overflow velocity increases. There is a

low pressure area in the opposite direction of jet. At the same time, the overflow impacts with the wall generating a higher pressure area^[22].

2.2.4 The Effect of Pressure on Flow Field

The boundary condition uses velocity inlet, which means that the greater the pressure is, the greater the velocity is. Therefore, studying the effect of velocity on the flow field can reflect the effect of pressure on the flow field. The boundary of the entrance speed are 100 m/s, 150 m/s, 200 m/s, observing the radial pressure distribution of nozzles. The radial pressure distribution of each nozzle at different inlet velocity is shown in Figure 8.

When the inlet velocity gets large, high speed jet can generate much higher pressure, but the distribution rule of radial pressure does not change and the position of low pressure area and high pressure area has not changed.

2.3 Rule of Particles Movement

2.3.1 The Track of Particles

Using discrete phase model, setting the properties, speed and concentration of particles, the track of particles is shown as below:

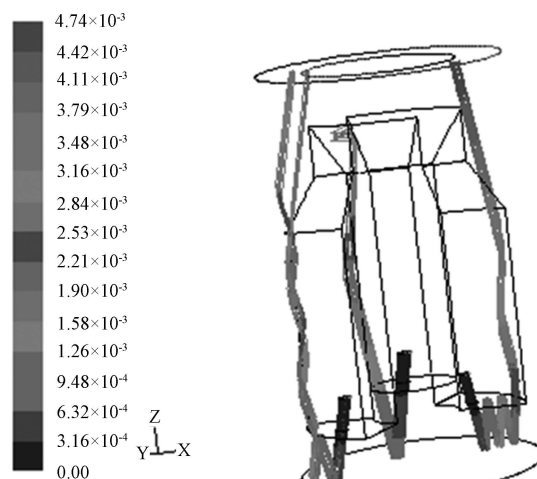


Figure 9
Track of Particles

From Figure 9, it can be seen that the particles mainly focus on the axis of nozzle and impacts rock at a higher speed generating great pressure. After the particle hits the rock, the speed of particle reduces greatly and particles run up. When particles impact with the bottom several times, particles flow into the annular space and thus are carried out.

2.3.2 Velocity Distribution of the Particle

At the beginning, the velocity of particle keeps invariant. The greater the diameter, the longer the particle speed keeps invariant. Then particle velocity gradually declines. Due to differences of the ejection angle and distance from the center of bit, particles impact with the bottom several times, which eject out from nozzle 1 and nozzle 2. After each impact, the energy losses greatly and the velocity reduces significantly. When particles eject out from nozzle 3, particles will flow into the annular space after an impact.

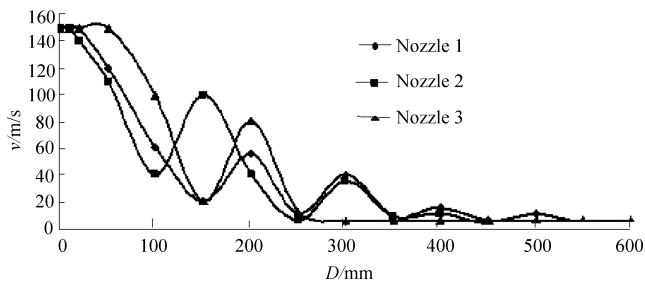


Figure 10
Particle Velocity Distribution of Nozzle

CONCLUSION

(a) The structure of the flow field can be roughly divided into five parts: Free jet area, impact area, overflow area, return area and vortex area.

(b) There must be a best distance, which can satisfy the need of speed, and also can get the best rock breaking effect.

(c) The jet impacts with the bottom and then generates high pressure clittella. The maximum pressure of nozzle 1 appears at 90 mm apart from the center of bit. The maximum pressure of nozzle 2 appears at 100 mm and the maximum pressure of nozzle 3 appears at 50 mm. The high-frequency impact of particles and the effect of high pressure jet can improve the efficiency of rock breaking.

(d) With the increase of jet angle, the radial maximum pressure reduces and the impact area expands.

(e) When the pressure gets large, high speed jet can generate much higher pressure, but the distribution of pressure does not change and the position of low pressure area and high pressure area has not changed.

(f) At the beginning, the velocity of particle keeps invariant and focus on the axial of nozzle. The greater the diameter, the longer the particle speed keeps invariant. Then particle velocity gradually declines. Finally, impacting the formation generates high pressure and then flows into the annular after several impacts.

REFERENCES

[1] Wu, K. S., Gu, J. F., & Kuang, Y. C. (2004). Comment on particle impact drilling technology. *Journal of Southwest Petroleum University (Science & Technology Edition)*, 30(2), 142-146.

[2] Zhang, Z. P., Li, G. S., & Niu, J. L. (2005). Effective mechanical and hydraulic ways promise higher penetration rate for deep drilling. *Proceedings of the 7th National Congress on Hydrodynamics and 19th National Conference on Hydrodynamics* (pp.71-73), Shanghai, China.

[3] Ma, Q. M., & Wang, R. H. (2005). Study of the down hole vibration drilling technique induced by hydro pulse. *Proceedings of the 7th National Congress on Hydrodynamics and 19th National Conference on Hydrodynamics* (pp.80-82), Shanghai, China.

[4] Li, G. S., Shen, Z. H., & Xu, Y. J. (2005). Advances in basic study on ultra-high pressure water jet assisted drilling. *Petroleum Drilling Techniques*, 33(5), 20-23.

[5] Du, Y. K., Wang, R. H., & Ni, H. J. (2009). Large eddy simulation of self-oscillation pulsed water jet drawing in annulus fluid. *Journal of Hydrodynamics (Ser. A)*, 24(4), 455-462.

[6] Tan, C. F., & Cai, J. L. (2003). Trial tests for full exert advantages of turbo-drill to improve ROP in deep wells. *Petroleum Drilling Techniques*, 31(5), 30-32.

[7] Zhang, Y. Y., Liu, Y. W., & Xu, Y. J. (2011). Drilling characteristics of combinations of different high pressure jet nozzles. *Journal of Hydrodynamics (Ser. B)*, 23(3), 384-390.

[8] Xu, Y. J., Zhou, C. L., & Qian, H. B. (2010). The study of laser rock breaking method and its application in well drilling. *Petroleum Drilling Techniques*, 38(4), 129-134.

[9] Tibbitt, G. A., & Galloway, G. G. (2008). Particle drilling alters standard rock-cutting approach. *World Oil*, (6), 37-44.

[10] Curlett, H. B., Sharp, D. P., & Gregory, M. A. (2002). *U. S. Patent No. 6386300 B1*. Washington, DC: U. S. Patent and Trademark Office.

[11] Xie, C. L., Yang, A. L., & Chen, K. M. (2003). Effect of hydraulic factors on flow field at bottom hole of rotating drill bit and hydraulic optimistic design. *Journal of Hydrodynamics (Ser. A)*, 18(6), 455-462.

[12] Liao, H. L., & Li, G. S. (2004). Fluid-structure Interaction of high pressure water jets impinging on rock. *Journal of Hydrodynamics (Ser. A)*, 19(4), 452-457.

[13] Wang, Z. M., Guo, X. L., & Li, M. (2009). Effect of drill-pipe rotation on borehole cleaning for extended reach well. *Journal of Hydrodynamics (Ser. A)*, 21(3), 366-372.

[14] Liu, Z., Hyun, B. S., & Kim, M. R. (2008). Experimental and numerical study for hydrodynamic characteristics of oscillating hydrofoil. *Journal of Hydrodynamics (Ser. A)*, 20(3), 280-287.

[15] Lao, Y. J., Wang, Z. D., & Zhang, Z. S. (2009). Experimental measurement and analysis on the wake vortex of oscillating flexible caudal fin. *Journal of Hydrodynamics (Ser. A)*, 24(1), 106-112.

[16] Chen, T. G., & Guan, Z. C. (2006). *Theory and technology of drilling engineering* (pp.166-211). Dongying, China: The Press of the University of Petroleum.

[17] Kubrak, E., Kubrak, J., & Rowinsk, P. M. (2008). Vertical velocity distributions through and above submerged, flexible vegetation. *Hydrological Sciences*, 53(4), 905-920.

[18] Eric, G. P, & Leonard, J. P. (2005). Detached-eddy simulation of high-Reynolds-number beveled-trailing-edge boundary layers and wakes. *Journal of Fluids Engineering*, 127(3), 897-906.

[19] Liefvendahl, M., & Fureby, C. (2006, December). *LES and DES of high Reynolds number wall bounded flows*. Paper presented the 44th AIAA Aerospace Sciences Meeting and Exhibition Reno, USA.

[20] Curlett, H. B., Sharp, D. P., & Gregory, M. A. (2003). *U. S. Patent No. 6581700 B2*. Washington, DC: U. S. Patent and Trademark Office.

[21] Zhang, Y. L. (2006). Destruction mechanism of rock on abrasive jet action. *Journal of Liaoning Technical University*, 25(6), 836-838.

[22] Tibbitts, G. A., Padgett, P. O., Curlett, H. B., & Harder, N. J. (2006). *U. S. Patent No. 2006/0027398 A1*. Washington, DC: U. S. Patent and Trademark Office.